Oxygen concentration and modeling thermal decomposition of a high-performance material: A case study of polyimide (Cirlex)

Aditya Ramgobin, Gaelle Fontaine, Serge Bourbigot

Oxygen Concentration and Modeling Thermal Decomposition of a High-Performance Material: A Case Study of Polyimide (Cirlex)

Aditya Ramgobin [1], Gaëlle Fontaine [2] and Serge Bourbigot [2]*

[1] Univ. Lille, CNRS, INRAE, Centrale Lille, UMR 8207 - UMET - Unité Matériaux et Transformations, F-59000 Lille, France, aditya.ramgobin@univ-lille.fr,

[2] Univ. Lille, CNRS, INRAE, Centrale Lille, UMR 8207 - UMET - Unité Matériaux et Transformations, F-59000 Lille, France, gaelle.fontaine@ensc-lille.fr

* Correspondence: serge.bourbigot@ensc-lille.fr

Abstract: Kinetic decomposition models for the thermal decomposition of a high-performance polymeric material (Polyimide, PI) were determined from specific techniques. Experimental data from thermogravimetric analysis (TGA) and previously elucidated decomposition mechanism were combined with numerical simulating tool to establish a comprehensive kinetic model for the decomposition of PI under three atmospheres: nitrogen, 2% oxygen, and synthetic air. Multi-staged kinetic models with subsequent and competitive reactions were established by taking into consideration the different types of reactions that may be occurring during the thermal decomposition of the material (chain scission, thermo-oxidation, char formation). The decomposition products and decomposition mechanism of PI which was established in our previous report allowed for the elucidation of the kinetic decomposition models. A three-staged kinetic thermal decomposition pathway was a good fit to model the thermal decomposition of PI under nitrogen. The kinetic model involved an autocatalytic type of reaction followed by successive nth order reactions. Such types of models were set up for the evaluation of the kinetics of the thermal decomposition of PI under 2% oxygen and in air, leading to models with satisfactory fidelity.

1. Introduction

31 Polyimide (Cirlex or Kapton, PI) is a high-performance polymeric material used in a
32 wide array of applications, due to its outstanding physical properties. Indeed,
33 polyimides are known to have exceptional thermal stability. This is attributed to their
34 rigid heterocyclic imide and aromatic rings on the polymer backbone[1]. They are used
35 in fields such as microelectronics, high temperature matrices, as well as for gas
36 separation membranes.

37 Previous work on the thermal stability and decomposition of polyimide has been
38 performed at our laboratory[2], whereby different behavioral traits of PI were
39 investigated. These traits involved the investigation of the thermal decomposition
40 mechanism under pyrolytic conditions, the incidence of oxygen concentration on the
41 thermal stability of PI, as well as the evaluation of the fire behavior of PI under
42 different heat fluxes using the mass loss cone calorimeter.

43 In our previous work, we have evidenced that the thermal behavior of PI is quite
44 different depending on the oxygen concentration. There are several stages involved
45 in the thermal decomposition of PI, and the stages differ greatly whether the thermal
46 stress is oxygen rich or deprived. Therefore, in order to complement the thermal
47 decomposition of PEEK in a fire scenario, kinetic models corresponding the
48 decomposition in oxygen-free, oxygen-poor, and oxygen rich (air) atmosphere need
49 to be investigated.

50 The TG and DTG plots of thermogravimetric analysis (TGA) performed on PI at
51 different oxygen concentrations (**Figure 1**) show that the initial degradation
52 temperature is not highly dependent on the oxygen concentration. However, it is
53 clear from the TG plots that at high temperatures, the role of oxygen in the thermal
54 decomposition of PI is significant. Indeed, at higher temperatures (above 600 °C),
55 the mass loss increases with increasing oxygen concentration. This suggests that
56 the thermal decomposition mechanism is also highly dependent on the oxygen
57 concentration, even if it is as low as 2%.

58 **Figure 1.** TG and DTG plots of PI heated at 10 °C/min under nitrogen, 2%, 4%, 8% and 12%, and in
59 air[2].

60 In order to further the understanding of the thermal decomposition characteristics of
61 PI, it was undeniably important to evaluate the kinetic parameters that govern its
62 thermal decomposition. In our previous work, we have observed that the presence
63 of oxygen may impact both the onset of the thermal decomposition and the char
64 degradation process[2].

65 Different oxygen concentrations correspond to different parts of a fire scenario.
66 Indeed, a material under a flame is scarcely in contact with oxygen because the
67 flame usually consumes all the oxygen in the surrounding environment. Therefore,
68 the decomposition behavior at this point corresponds to solely pyrolytic effects.

69 However, if there is the presence of only a small flame, there may be some oxygen
70 (much lowered concentration as compared to air, as low as 2%) that is in contact
71 with the material. Furthermore, if the material is found away from a flame in a well-
72 ventilated environment, it subjected to thermal stress in the presence of air. Thus,
73 modelling the three oxygen levels may provide an integral insight on the
74 decomposition behavior of a burning material.

75 Therefore, it was of interest to evaluate the kinetic parameters of the thermal
76 decomposition of the material under three different oxygen concentrations: 0%, 2%,
77 and 20% (synthetic air).

78 **2. Materials and Methods**

79 Polyimide (Cirlex CL) was purchased from Goodfellow Cambridge Limited
80 (Huntington, England)

81 *2.1. Thermogravimetric Analysis (TGA)*

82 Thermogravimetric analyses (TGA) were conducted on a Netzsch Libra instrument.
83 Powdered samples of 9 - 10 mg (according to the good practice of TGA, it is
84 assumed the samples are thermally thin) were placed in open alumina pans and
85 heated up to 900 °C under different percentages of oxygen and nitrogen at different
86 heating rates (1, 2, 5, and 10 °C/min) up to 900 °C under 0%, 2%, and 20 % oxygen
87 concentrations.

88 *2.2. Kinetic Analysis*

89 Kinetic analysis and modeling of the degradation of the samples were made using a
90 Kinetics Neo software package developed by Netzsch Company. The principle has
91 been discussed by Opfermann in[3] and here we only briefly remind the reader of the
92 basic concepts of the method.

93 For kinetic analysis, it is assumed that the material decomposes according to Eq.
94 (1):

95 $$A_{solid} \rightarrow B_{solid\ or\ liquid} + C_{gas} \tag{1}$$
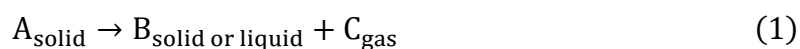
96 The rate expression de/dt, where e is the concentration of educt (reactant), is
97 assumed to be defined by Eq. (2):

98 $$\frac{de}{dt} = k(T) \times f(e, p) \tag{2}$$

99 Where k is the kinetic constant, p is the concentration of the product, $k = A\exp(-$
100 $E/RT)$ according to the Arrhenius law, A is the frequency factor, E is the activation
101 energy and f(e,p) is the so-called ''reaction equation'' or in the case of TGA, the
102 ''reaction model''.

103   All reactions are assumed to be irreversible. In the case of degradation and since
104   the evolved gases are continuously removed by the fluid flow in the TGA chamber,
105   this is a reasonable assumption. It is also assumed that the overall reaction (Eq. (9))
106   is the sum of individual reaction stages (formal or true stage) with constant activation
107   energy, as generally accepted in chemistry. The model can then include competitive,
108   independent and successive reactions. The equations are solved with multivariate
109   kinetic analysis (determination of the parameter via a hybrid normalized Gauss-
110   Newton method or Marquardt method)[4].

111   By optimizing the models used for the kinetic analysis, the kinetic parameters of each
112   stage in the thermal decomposition model of the material can be evaluated, allowing
113   for a better understanding of the thermal decomposition behavior of the material.

114   The approach used to model the decomposition behavior of PEEK was similar to
115   that adopted by Moukhina et al, whereby a model free analysis was used to
116   determine the initial kinetic decomposition parameters and gain insight regarding the
117   number of stages involved and the types of kinetic models that govern the
118   decomposition[5]. To this approach, we added our own understanding of the thermal
119   decomposition based our previous work on the same material[2], whereby the thermal
120   decomposition mechanism was attempted.

121   The reflection behind the methodology that we have adopted is briefly summarized
122   hereunder.

123   In order to model the kinetic degradation of a polymeric material, two separate
124   functions can be assumed. One being temperature dependent (K(T)), and the other
125   governed by the conversion, α, f(α). The latter can be of any value from 0 (no
126   degradation) to 1 (complete degradation). Therefore, the differential equation that
127   defines the kinetics of thermal degradation can be written as equation 3[6].

128
$$\frac{d\alpha}{dt} = K(T)f(\alpha) \tag{3}$$

129    $\frac{d\alpha}{dt}$ is the rate of degradation, K(T) is the temperature dependent rate constant, and

130    $f(\alpha)$ corresponds to the reaction model. $K(T)$ can be described by the Arrhenius
131   equation (equation 4):

132
$$K(T) = Ae^{-\left(\frac{E}{RT}\right)} \tag{4}$$

133   Where R is the universal gas constant, E, the activation energy, and A, the pre-
134   exponential factor[7].

135 The time dependence of equation (4) can be eliminated by using a constant heating

136 rate $\beta = \frac{dT}{dt}$, by dividing by it (equation 5).

$$\frac{d\alpha}{dT} = \frac{A}{\beta} f(\alpha) e^{-\frac{E}{RT}} \tag{5}$$

138 Linearizing equation 5 leads to obtainable kinetic parameters (A and E) by using the
139 equation 6.

$$\ln\left(\frac{\frac{d\alpha}{dT}}{f(\alpha)}\right) = \ln\left(\frac{A}{\beta}\right) - \left(\frac{E}{RT}\right) \tag{6}$$

141 One approach for kinetic modelling involved the assumption that the activation
142 energy and the preexponential factor are constant. A well-known technique that uses
143 this method is the Friedman method, whereby the activation energy and pre-
144 exponential factor are obtained by plotting the logarithmic form of the rate equation
145 of each heating rate (equation 3). α represents the value at a certain degree of
146 conversion, and i the data from the corresponding heating rate experiment[8].

$$\ln\left[\beta_i\left(\frac{d\alpha}{dT}\right)_{\alpha,i}\right] = \ln\left(A_\alpha f(\alpha)\right) - \frac{E_\alpha}{RT_{\alpha,i}}) \tag{7}$$

148 The activation energy at particular conversion degrees can be calculated with linear

149 regression from a plot of $\ln\left[\beta_i\left(\frac{d\alpha}{dT}\right)_{\alpha,i}\right]$ against $\frac{1}{T_{\alpha,i}}$ for the heating rates that were

150 used. The plot can provide confirmation as to whether there is more than one stage
151 involved in the degradation process. Moreover, the nature of the decomposition
152 stage can also be deduced by comparing the slope of a constant heating rate data[9].
153 By comparing the magnitudes at the peak slope (the one that is on the right side of
154 the peak) and that of isoconversion lines, three types of reactions are defined:
155 normal, accelerated, and retarded (**Figure 2**).

156 **Figure 2.** Friedman plots corresponding to a normal type of reaction (left), an accelerated reaction
157 (middle), and a retarded reaction (right).[9]

158 A normal reaction corresponds to the curve whereby the magnitude of the peak slope
159 (slope to the right of the peak) and that of the isoconversion lines are of the same
160 magnitude. An accelerated reaction is one whereby the peak slope is steeper than
161 that of the isoconversion lines. Contrarily, a retarded reaction has a peak slope which
162 is gentler than that of the isoconversion lines. However, one of the major limitations
163 of this method is that it does not cater for the possibility of competitive parallel
164 reactions that may occur during the thermal decomposition process.

165 It should be noted that for the reaction model to make physical sense, reaction orders
166 above three are not considered. However, because of the complexity of the reactions
167 occurring during the thermal decomposition of a polymeric material, optimizations
168 based on experimental data can lead to non-integer values of reaction orders. This
169 often happens when a stage involves more than one pathway towards the same
170 decomposition product.

171 Another similar method that is used for model free analyses of kinetic degradation is
172 the Ozawa-Flynn-Wall integral isoconversional method[10,11].

173 The Ozawa-Flynn-Wall analysis involves an integral method for the calculation of the
174 kinetic parameters, therefore, there is no separation of variables involved. As a
175 result, competitive reactions show variations in activation energies between the
176 Ozawa-Flynn-Wall and the Friedman analyses[9]. This will be helpful in determining
177 the nature of the stages involved in the thermal decomposition of the materials
178 investigated.

179 Moreover, the insight regarding the thermal decomposition behavior of the polymeric
180 materials will be used in order to devise an experiment-based model, aided by the
181 model free analysis detailed above.

182 There are several reaction types that can be attributed to a decomposition stage.
183 The typical homogenous reactions and classic solid reactions are listed in **Table 1**.

184 The models were optimized using the KineticsNeo software (Netzsch). We have
185 attempted to make kinetic models with the lowest number of stages that gave an
186 acceptable fit and that were consistent with the thermal decomposition mechanism
187 of the material studied.

188   **Table 1**. Reaction types and corresponding reaction equations $\frac{d\alpha}{dt} = -A\, e^{\frac{E}{RT}} f(\alpha)$

189 **3. Results and Discussion**

190 *3.1. PI decomposition in nitrogen*

191 TG curves and their corresponding DTG curves when PI is subjected to four different
192 heating rates under nitrogen are shown on **Figure 3**.

193   **Figure 3.** TGA (left) and the corresponding DTG (right) curve of PI at 1 (black), 2 (red), 5 (blue), and
194   10 K/min (magenta), under nitrogen.

195 From the TGA plots of PI (**Figure 3**), it is clear that PI has a high thermal stability as
196 hardly any mass loss is recorded until almost 500 °C. he temperature at the onset of
197 the decomposition increases with increasing heating rate. It involves an apparent
198 sharp decomposition stage, whereby around 30 wt% of mass loss is observed. This
199 decomposition can be seen as the first peak on the DTG curve. After this peak, the

200 mass loss rate decreases, but only to around 0.5 wt%/°C. This suggests that there
201 is another stage involved in the thermal decomposition of PI.

202 It can be noted that the maximum mass loss rate decreases with increasing heating
203 rate. This suggests that the first decomposition stage follows the same kinetic
204 pathway. To further the understanding of the kinetics of the thermal decomposition
205 behavior, the model free analysis (Friedman analysis) was performed on the TGA
206 curves of PI at the different heating rates. The Friedman plot as well as the
207 isoconversion lines corresponding to different conversions are plotted on **Figure 4**.

208 **Figure 4.** Friedman analysis of PI using 4 different heating rates under nitrogen (orange: 1 K/min,
209 green: 2 K/min, red: 5 K/min, blue: 10 K/min)

210 From the Friedman analysis (**Figure 4**), it can be observed that the isoconversion
211 lines to the right of the first peak has a gentler slope than the slope of the peaks.
212 This means that the first decomposition reaction is accelerated. This is often the case
213 in polymeric materials because their decomposition leads to the generation of
214 radicals which are very reactive and contribute to the further decomposition of the
215 material. For this reason, the first stage of the thermal decomposition was assigned
216 to an autocatalytic decomposition rate model (Cn).

217 Moreover, the activation energy and pre-exponential factor based on the model free
218 Friedman analysis is shown on **Figure 5**.

219 **Figure 5.** Activation energy plot for PI under nitrogen, obtained by Friedman analysis

220 From the two plots on **Figure 5**, it can be seen that the activation energy and the
221 pre-exponential factor are relatively constant at the beginning of the decomposition
222 process, until around 60% of conversion. After this, the activation energy increases
223 rapidly from around 300 to around 1400 kJ/mol at 100% conversion. This means that
224 there are at least two stages in the thermal decomposition of PI under nitrogen.
225 Moreover, at around 90% conversion, there seems to be a slight change in the
226 continuity of the curve, suggesting that there might be another step in the
227 decomposition reaction. In order to check whether there are any competitive
228 reactions occurring, the activation energies calculated from an Ozawa-Flynn-Wall
229 curve was plotted on the same axes as the activation energies from the Friedman
230 plot. This graph is shown on **Figure 6**.

231 **Figure 6.** Activation energies calculated using Friedman analysis (black) and the Ozawa-Flynn-Wall
232 method (magenta) for PI under nitrogen

233 By comparing the evolution of the activation energies calculated from the two
234 aforementioned methods, it can be seen that for the first 50% of the conversion,
235 there is very little difference in activation energy. This means that there are not

competitive reactions in the first step of the thermal decomposition. However, at higher conversions, we can see that the activation energies curves do not have the exact same shape, but the values are only slightly different.

From the model free analyses, we have seen that there are at least three stages in the thermal decomposition of PI under nitrogen. Additionally, the comparison of the activation energies from the derivative model free analysis (Friedman) and the integral model free analysis (Ozawa-Flynn-Wall), we have deduced that there are not competitive reactions occurring during the thermal decomposition. Moreover, it was seen from both the activation energy plots that towards the end of the conversion, the activation energy of the thermal decomposition increases greatly.

These inputs are essential for the elaboration of a kinetic model for the thermal decomposition mechanism of PI. The model that was chosen is illustrated on **Scheme 1** and explained in the subsequent paragraphs.

Scheme 1. Kinetic model used to model the thermal decomposition kinetics of PI under nitrogen

Moreover, in the mechanism of the thermal decomposition of PI that was detailed in our previous work[2], the different reactions occurring during the thermal breakdown of PI under nitrogen are also known. The first stage of the decomposition involves the random scission of the polymer chain. This corresponds to the first decomposition stage, which is also the main decomposition stage of the thermal decomposition. The kinetic model that was used for this stage of the decomposition corresponds to an autocatalytic reaction. Indeed, the random scission of a polymeric chain leads to the formation of reactive radicals that often take part in the subsequent decomposition of a material.

After the random scission of the polymeric chains, small amounts of gases such as ammonia, hydrogen cyanide, and methane gave off and were characterized by TGA connected to Fourier Transform Infrared (FTIR). The formation of methane and hydrogen cyanide probably comes from the secondary decomposition of aromatics that are formed during the char formation process. Indeed, at high temperatures, the char continues to strengthen and degrade, releasing hydrogen and low molecular weight products such as methane. This corresponds to part of the second stage of the decomposition of PI under nitrogen.

Furthermore, the presence of hydrogen (which is assumed by the presence of methane), means that nitrogen containing moieties may be reduced to ammonia at high temperatures. This explains the slightly delayed detection of ammonia in the TGA-FTIR [2], and corresponds to the third stage. **Table 2** shows the kinetic parameters that were optimized for the decomposition model.

Table 2. Kinetic parameters used in the model for the thermal decomposition of PI under nitrogen

273   The last two stages correspond to extremely high activation energies, which is
274   coherent with both the Friedman and the Ozawa-Flynn-Wall methods. However, the
275   exact reactions occurring at such high temperatures are unknown. This is because
276   the exact structure of the char formed during the initial decomposition is not perfectly
277   known. However, we can safely mention that the 3-stage reaction is coherent with
278   the release of the decomposition products that were identified.

279   The first stage of the decomposition was assigned to an autocatalytic decomposition,
280   with an activation energy around 278 kJ/mol, a reaction order of 3.00 and an
281   autocatalytic order of 0.377. This activation energy is coherent with the Friedman
282   analysis **Figure 5**. The two subsequent reactions were modeled as Arrhenius
283   reactions, with activation energies of 370 and 410 kJ/mol, respectively. This
284   corresponds to the high activation energy seen for the decomposition at conversions
285   superior to 60%. These two reactions correspond to the slow decomposition of the
286   char formed during the first stage of the decomposition and each share around 20%
287   of contribution to the whole mechanism.

288   Moreover, from **Table 2**, it can be seen that the first decomposition stage, which
289   corresponds to the autocatalytic stage, is the one that has the highest contribution.
290   The other two stages are also kinetically significant, with contributions of around 19%

291   From the kinetic parameters in **Table 2**, the best fit model of mass loss with
292   temperature was plotted along with the experimental TGA curves. The resulting
293   graph is shown on

294   **Figure 7**.

295   **Figure 7.** Best fit of the TG data for the three-stage reaction models in **Scheme 1**, with the parameters
296   given on **Scheme 1**. The curves represent the experimental data and the symbols represent the model

297   From a statistical point of view, the correlation coefficient of the model with respect
298   to the experimental data was 0.99964.

299   From the model that was adopted, the major decomposition reaction corresponds to
300   the first stage, with a contribution of 62.5 % in the model. However, the subsequent
301   stages have a non-negligible contribution (18.8 %) to the model. This means that the
302   char decomposition plays a major role in the thermal decomposition model of PI.

303   Having the kinetics of the decomposition of PI under nitrogen in hand, our interest
304   went to the effect that oxygen may have on kinetics of the thermal decomposition of
305   PI. Therefore, the thermal behavior of PI under 2% oxygen was studied and is
306   detailed in the next section.

307   *3.2. PI decomposition in 2% oxygen*

To model the kinetic decomposition of PI under 2% oxygen, dynamic TGA was performed on PI at low oxygen levels at different heating rates. The resulting TG curves and their corresponding DTG curves of PI under 2% oxygen are shown on **Figure 8**.

Figure 8. TGA (left) and the corresponding DTG (right) curve of PI at 1 (black), 2 (red) ,5 (blue), and 10 K/min (magenta), under 2% oxygen

Quite expectedly and similarly to the initial investigation of PI under different oxygen levels, PI remains stable up to a relatively high temperature of around 450 °C. From the TG curves it appears that there is only one decomposition stage in the thermal decomposition of PI under 2% oxygen. Nevertheless, when looking at the DTG curves for heating rates corresponding to 2, 5, and 10 K/min, there seems to be at least two peaks for the thermal decomposition of PI. The absence of a visible second peak at the heating rate of 1K/min is assigned to the two decomposition stages occurring at similar temperature ranges.

Therefore, from the TGA and DTG curves, we can deduce that the thermal decomposition mechanism of PI is at least a two-stage process. To confirm this, Friedman analysis was performed on the data from the above TG curves. The resulting plot is shown in **Figure 9**.

Figure 9. Friedman analysis of PI using 4 different heating rates under 2% oxygen (orange: 1 K/min, green: 2 K/min, red: 5 K/min, blue: 10 K/min)

The Friedman plot shows a small peak at the beginning of the decomposition, followed by another at around 50% conversion. Finally, another decomposition stage is visible towards 100% conversion. This peak is not visible in the Friedman plot at 10 K/min. This may be because at the maximum temperature of the TG experiment, the mass loss was not total, suggesting that the reaction had not reached its completion. From these plots, we can deduce that there are at least three stages involved in the thermal decomposition of PI under 2% oxygen.

From this Friedman plot, the activation energies as well as the pre-exponential factor for the decomposition of PI was plotted with respect to the conversion (**Figure 10**). This is essential to obtain initial parameters for the modeling of the thermal decomposition of PI.

Figure 10. Activation energy plot for PI under 2% oxygen, obtained by Friedman analysis

From this Friedman plot, it can be seen that at low conversion, the activation energy is relatively high (around 350 kJ/mol). This corresponds to the first stage of the decomposition. However, as the material decomposes further, the activation energy decreases rapidly and is dependent on the conversion degree. This is assigned to the second stage of the thermal decomposition. At conversions above 70%, the

345 activation energy is still dependent on the conversion, but unlike the previous stage,
346 it seems to increase slightly. This is assigned to the third stage of the decomposition.

347 Based on the two Friedman analysis plots, we have seen that the thermal
348 decomposition of PI under 2% oxygen corresponds to at least three stages of
349 decomposition. In order to have insight concerning eventual competitive reactions
350 that might be occurring during the decomposition of PI, the activation energy based
351 on calculations using Friedman analysis was compared to that based on the OFW
352 method (**Figure 11**). Because of the difference in the approach for the two similar
353 methods, the occurrence of competitive reactions is translated by a difference in
354 activation energy for the same conversion.

355

356 **Figure 11.** Activation energies calculated using Friedman analysis (black) and the Ozawa-Flynn-Wall
357 method (magenta) for PI under 2% oxygen

358 From the two activation energy plots, it can be seen that the global shapes of the
359 two activation energy plots are relatively similar. Indeed, the activation energy
360 increases for early conversions and then decreases. The increase in activation
361 energy can be assigned to the breaking of chemical bonds (endothermic) which
362 generate radicals. The following decrease in activation energy is assigned to
363 recombination reactions between radicals which potentially lead to the formation of
364 a stable char (exothermic).

365 Moreover, there is a slight difference in the activation energy for the first stage of
366 decomposition. However, the error is significant for the first stage of the
367 decomposition. It is therefore hard to conclude whether the competitive stage occurs
368 during the first stage or later. As a result, the kinetic decomposition model was based
369 on the understanding of chemical reactions occurring at the onset of the
370 decomposition.

371 The model free analyses have provided insight on the number of stages that are
372 involved in the thermal decomposition of PI. Using knowledge acquired from the
373 thermal decomposition of PI in our previous work[2], kinetic model for the thermal
374 decomposition of PI under 2% oxygen is suggested (Scheme 2).

375 **Scheme 2**. Kinetic model used to model the thermal decomposition kinetics of PI under 2% oxygen

376 Similarly to the decomposition of PI under nitrogen, a three-stage pathway was used
377 to model the thermal decomposition of PI under 2% oxygen. However, in order to
378 involve the thermo-oxidation reactions in the model, a supplementary stage was
379 required. From the TGA of PI under varying oxygen concentrations[2], it was seen that
380 oxygen intervenes right at the start of the decomposition. Therefore, the thermo-

381   oxidation stage was added as a competitive reaction at the very first stage of the
382   decomposition model (stage 1.2).

383   The optimized kinetic parameters for the thermal decomposition of PI under 2%
384   oxygen are summarized in **Table 3**.

385   **Table 3.** Kinetic parameters used in the model for the thermal decomposition of PI under 2 % oxygen

386   The optimized parameters for the kinetic model fit well with the experimental TG
387   curves (**Figure 12**). The activation energy for the two competitive reactions at the
388   beginning of the reaction are of the same order of magnitude. One of the two
389   reactions from the first stage of the decomposition is assigned to the thermal
390   decomposition of PI, while the other one is assigned to the thermo-oxidation of the
391   polymer backbone.

392   Since thermo-oxidation usually results in the formation of carbon dioxide, carbon
393   monoxide and water, no subsequent reaction is assigned after the reaction
394   corresponding to the thermo-oxidation of the polymer backbone.

395   The second stage is assigned to the subsequent thermal decomposition of the
396   decomposition products formed during the initial thermal decomposition. Indeed,
397   from the previous study, we have concluded that the first decomposition of PI may
398   lead to the formation of a thermally stable char, or another crosslinked structure.

399   The formation of this structure is aided by the presence of radicals resulting from the
400   initial decomposition reactions (stage 1.1). Moreover, this structure may further
401   thermally decompose into smaller structures. This leads to the formation of more
402   radicals that can in turn participate in furthering the decomposition. Therefore, the
403   second stage of the decomposition of PI was assigned to an autocatalytic reaction
404   type. This stage has a relatively low activation energy because of the presence of
405   radicals that are still lingering around the polymer after the first decomposition stage.
406   Moreover, these recombination reactions eventually lead to stable char formation as
407   it was seen in our previous work dealing with the decomposition mechanism of PI.[12]
408   Char formation reactions are exothermic and could also explain the lowering of the
409   activation energy on the activation energy plot on **Figure 10**.[13]

410   The last reaction stage corresponds to the thermo-oxidation of the remaining organic
411   material and carbonaceous char.

412   **Figure 12.** Best fit of the TG data for the three-stage reaction models in **Scheme 2**, with the
413   parameters given on **Table 3**. The curves represent the experimental data and the symbols represent
414   the model.

415   When comparing with the decomposition model under nitrogen, an additional
416   competitive decomposition reaction is observed in the first stage of the thermal
417   decomposition model of PI under low oxygen concentration. This is because thermo-

418 oxidation occurs right at the beginning of the decomposition of PI, parallelly to
419 pyrolytic decomposition. It is interesting to note that these two initial decomposition
420 reactions have a significant contribution to the decomposition. Indeed, about 50 %
421 of the model is assigned to the two initial stages. The other decomposition stages
422 correspond to the char degradation and oxidation. Moreover, from a statistical point
423 of view, the correlation coefficient between the experimental curve and the simulated
424 curve based on the kinetic model is 0.99949., meaning that the model used to
425 simulate the thermal decomposition of PI under 2% oxygen is consistent with the
426 experimental TG curves.

427 To complete the investigation of the kinetics of the thermal decomposition of PI under
428 different oxygen concentrations, the behavior of PI in air was also investigated.

3.3. PI decomposition in air

430 After having investigated the thermal decomposition behavior of PI under low oxygen
431 concentrations the kinetic of the thermal decomposition of PI in air was studied so
432 that the effect of a highly thermo-oxidative atmosphere can be better understood.
433 This also allows for the simulation of the degradation behavior when the material is
434 subjected to heat in a well-ventilated environment. The presence of oxygen in air
435 usually increases the extent to which a material decomposes when under thermal
436 stress. Sometimes, oxygen can have a catalytic effect on the onset of the
437 decomposition of a material.

438 Dynamic TGA was used to investigate the kinetics of the thermal decomposition
439 behavior of PI in air. The TG curves of PI and their corresponding DTG curves at
440 four different heating rates are shown on **Figure 13**.

441 **Figure 13.** TGA (left) and the corresponding DTG (right) curve of PI at 1 (black), 2 (red) ,5 (blue), and
442 10 K/min (magenta), in air.

443 From the TG curves of PI in air, it can be seen that the thermal stability of PI is
444 maintained until around 450 °C, whereby the onset of thermal decomposition is
445 observed at the beginning of a mass loss process. The TG curves all appear to follow
446 an apparent single stage. However, on the DTG curves, at high heating rates, a
447 second peak, which is close to the first, is noticeable. This means that the kinetics
448 of the thermal decomposition of PI in air occurs in at least two stages. In order to
449 obtain further information regarding the number of stages and the types of reactions
450 occurring during the thermo-oxidative decomposition of PI in air, the Friedman plot
451 for the corresponding heating rates was plotted (**Figure 14**).

452 **Figure 14.** Friedman analysis of PI using 4 different heating rates in air (orange: 1 K/min, green: 2
453 K/min, red: 5 K/min, blue: 10 K/min)

454   From the Friedman plot, an accelerated decomposition stage can be distinguished
455   as a first peak. The peak slope is steeper than the isoconversion lines. This suggests
456   that the first decomposition stage is accelerated, probably autocatalytic[9]. At higher
457   heating rates (5 and 10 K/min) there seems to be another peak that is visible right
458   after the first one. This confirms that there are at least two stages in the thermal
459   decomposition of PI in air. it is therefore likely that at low heating rates, the two
460   thermal decomposition stages are overlapping.

461   In order to see any eventual reactions that may be occurring during the thermo-
462   oxidative decomposition of PI, the activation energy and log(pre-exponential factor)
463   (calculated from the Friedman analysis), was plotted with respect to the conversion
464   (**Figure 15**).

465   **Figure 15.** Activation energy plot for PI in air, obtained by Friedman analysis

466   The activation energy is relatively high at the beginning of the conversion (around
467   190 kJ/mol). It decreases until around 60% conversion where the activation energy
468   is at around 130 kJ/mol. This means that there is another stage in the decomposition
469   of PI. At this point, and until almost 98 % conversion, there is little evolution in the
470   activation energy. At 100% conversion, there is a high increase in activation energy.
471   However, the error at this conversion is very high, therefore, it was not taken into
472   consideration as a subsequent decomposition stage.

473   The activation energy plot based on the Friedman method provided out the number
474   of consecutive stages occurring during the thermo-oxidative decomposition of the
475   material. To further the understanding of decomposition in terms of competitive
476   reactions that may occur, the activation energy plot based on the Friedman method
477   was compared with that based on the OFW method (**Figure 16**).

478   **Figure 16.** Activation energies calculated using Friedman analysis (black) and the Ozawa-Flynn-Wall
479   method (magenta) for PI in air.

480   From the two activation energy plots on **Figure 16**, it can be seen that the two
481   methods lead to very different activation energies in at around 50% conversion. This
482   strongly suggests that there are competitive reactions occurring during the thermal
483   decomposition of PI in air. It was therefore considered when elaborating the kinetic
484   model for the thermo-oxidative decomposition of PI.

485   Based on knowledge acquired during the investigation of the thermal stability of PI
486   and its thermal decomposition mechanism under nitrogen, we were able to take an
487   attempt at defining a kinetic model for the thermo-oxidative decomposition of PI in
488   air. The model is shown on **Scheme 3**.

489   **Scheme 3.** Kinetic model used to model the thermal decomposition kinetics of PI in air.

490   From **Scheme 3**, two major consecutive decomposition stages are illustrated. The
491   first corresponds to the initial decomposition of PI, similarly to the thermal
492   decomposition of PI under nitrogen. It corresponds to the random scission of the
493   polymer backbone. However, it was observed that the presence of oxygen tends to
494   slightly decrease the thermal stability of PI at high temperatures[2]. This translates into
495   a lower activation energy for the onset of the decomposition. Additionally, the initial
496   decomposition leads to the formation of reactive radicals which can take part in the
497   scission of the initial polymer. This effect can be assigned to an autocatalytic type of
498   decomposition reaction whereby the products increase the rate of the
499   decomposition. During this stage, rearrangement of the polymer backbone to form a
500   crosslinked char structure was also hypothesized under nitrogen. This char is highly
501   stable under inert atmosphere, but not under oxygen. This was evidenced by the
502   TGA under different oxygen levels, whereby the second decomposition of PI was
503   largely affected by the presence of oxygen.

504   It was therefore not unexpected to add a stage whereby the thermo-oxidative
505   reactions are occurring. This corresponds to stage 2.2. Furthermore, while the
506   material is being thermo-oxidized, there are also thermal decomposition that is on-
507   going, via a similar mechanism as the first stage. However, the initial structure of the
508   polymer has changed, and so have the kinetic parameters for the decomposition
509   stage. Therefore, an autocatalytic type decomposition mechanism was assigned to
510   this stage.

511   The optimized kinetic parameters used in for the modeling of the thermal
512   decomposition of PI in air are summarized in **Table 4**.

513   **Table 4.** Kinetic parameters used in the model for the thermal decomposition of PI in air

514   The activation energy for the first decomposition stage is coherent with the activation
515   energy calculated using the Friedman analysis for the first stage (**Figure 15**). This
516   first stage of thermal decomposition formed a charred structure and possibly a
517   partially decomposed form of the polymer. Further thermal decomposition of this
518   structure is modeled by reaction 2.1. This was assigned to a similar reaction as the
519   first decomposition stage. However, since the chains have already partially been
520   broken, the activation energy is lower. Moreover, in the presence of air, the structure
521   undergoes thermo-oxidation (modeled by reaction 2.2).

522   The simulated TG curves based on the kinetic model above as well as the
523   experimental TG curves are shown on **Figure 17**.

524   **Figure 17.** Best fit of the TG data for the three-stage reaction models in **Scheme 3**, with the
525   parameters given on **Table 4**. The curves represent the experimental data and the symbols represent
526   the model.

527 Contrarily to the kinetic model of the thermal decomposition of PI under 2% oxygen,
528 the model in air does not have competitive reactions in the initial decomposition
529 stage. However, the autocatalytic nature of the reaction model suggests that there
530 are reactive decomposition products that are released during that stage, leading to
531 the formation of a char as well as releasing oxidation products. Moreover, the other
532 two decomposition reactions have been assigned to two thermo-oxidation reactions,
533 each with a significant contribution as compared to the first stage of the
534 decomposition. Indeed, the decomposition of the char (stage 2.2) and the further
535 thermo-oxidation of the polymer (stage 2.1) play a bigger role in the thermal
536 decomposition than the initial char formation reaction (stage 1). It is interesting to
537 note that the thermo-oxidation of the char corresponds to a low order kinetic reaction
538 model (reaction order = 0.06). This means that it is only slightly dependent on the
539 "concentration" of the reactants.

540 The fitted curve seems to correspond well with the experimental curve. From a
541 statistical point of view, the correlation coefficient between the experimental and the
542 simulated curve is 0.99993.

4. Discussion and Conclusion

544 The kinetic parameters for the thermal decomposition of PI under three different
545 oxygen levels have been calculated. We have seen that, from a kinetic perspective,
546 the decomposition pathway adopted by PI during its thermal decomposition is
547 significantly dependent on the oxygen concentration.

548 Under nitrogen, the kinetic pathway adopted during its thermal decomposition is
549 relatively simple. However, the presence of a small amount of oxygen brings about
550 a significant change in kinetic pathway adopted by the material during its thermal
551 decomposition. Indeed, in the presence of a small concentration of oxygen, the
552 decomposition pathway is much complexified, leading to a 3-stage decomposition
553 involving a competitive reaction at the initial decomposition stage. Moreover, it was
554 reported that the presence of oxygen increases the crosslinking that occurs in a
555 material [14]. This can be extrapolated to PI, which is also a highly charring polymeric
556 material. Therefore, the higher activation energy that is observed for the thermal
557 decomposition of PI under low oxygen concentration suggests that major
558 crosslinking would have had occurred during the initial decomposition reactions.

559 Under air, the activation energy for the onset of the decomposition is lower than
560 under pyrolytic conditions. One explanation for this can be that decomposition gases
561 that are produced at the beginning of the decomposition are readily oxidized. A fast
562 consumption of the decomposition gases pulls the kinetics towards the further
563 decomposition of the material. Moreover, the presence of recombination reactions
564 within the polymeric matrix may also be occurring owing to the charring properties of

565 the polymer can also explain the lowered activation energy due to their exothermic
566 nature.

567 We have seen that from a kinetics perspective, the pathway adopted by PI during its
568 thermal decomposition is highly dependent on the oxygen concentration. Moreover,
569 low oxygen concentration leads to a higher crosslinking, leading to an increase in
570 the activation energy of the onset of decomposition. However, in air, the crosslinking
571 is taken over (for the most part), by thermo-oxidation. The difference in the kinetics
572 of the thermal decomposition of PI has provided deep insight on the eventual
573 behavior of the material under a fire scenario.

574

579 **Conflicts of Interest:** The authors declare no conflict of interest.

580

581

5. References

1. Ramgobin A, Fontaine G, Bourbigot S. Thermal Degradation and Fire Behavior of High Performance Polymers. *Polym Rev.* 2019;59(1):55-123. doi:10.1080/15583724.2018.1546736

2. Ramgobin A, Fontaine G, Bourbigot S. Investigation of the thermal stability and fire behavior of high performance polymer: A case study of polyimide. *Fire Saf J.* 2020;(April):103060. doi:10.1016/j.firesaf.2020.103060

3. Opfermann J. Kinetic analysis using multivariate non-linear regression. I. Basic concepts. *J Therm Anal Calorim.* 2000;60(2):641-658. doi:10.1023/A:1010167626551

4. Kaisersberger E, Opfermann J. Kinetic evaluation of exothermal reactions measured by DSC. *Thermochim Acta.* 1991;187(C):151-158. doi:10.1016/0040-6031(91)87189-4

5. Moukhina E. Determination of kinetic mechanisms for reactions measured with thermoanalytical instruments. *J Therm Anal Calorim.* 2012;109(3):1203-1214. doi:10.1007/s10973-012-2406-3

6. Kinetics SR. Chapter 3 Theory of Solid State Reaction Kinetics. *Compr Chem Kinet.* 1980;22(C):41-113. doi:10.1016/S0069-8040(08)70384-4

7. Vyazovkin S. Kinetic concepts of thermally stimulated reactions in solids: A view from a historical perspective. *Int Rev Phys Chem.* 2000;19(1):45-60. doi:10.1080/014423500229855

8. Friedman HL. Kinetics of Thermal Degradation of Char-Forming Plastics from Thermogravimetry . Application to a Phenolic Plastic. (6):183-195.

9. Hondred PR, Yoon S, Bowler N, Moukhina E, Kessler MR. Degradation kinetics of polyimide film. *High Perform Polym.* 2011;23(4):335-342. doi:10.1177/0954008311409262

10. Ozawa T. A New Method of Analyzing Thermogravimetric Data. *Bull Chem Soc Jpn.* 1965;38(11):1881-1886. doi:10.1246/bcsj.38.1881

11. Flynn JH, Wall LA. A quick, direct method for the determination of activation energy from thermogravimetric data. *J Polym Sci Part B Polym Lett.* 1966;4(5):323-328. doi:10.1002/pol.1966.110040504

12. Ramgobin A, Fontaine G, Bourbigot S. Investigation of the thermal stability and fire behavior of high performance polymer: A case study of polyimide. *Fire Saf J.* 2020;(May). doi:10.1016/j.firesaf.2020.103060

13. Li J, Stoliarov SI. Measurement of kinetics and thermodynamics of the thermal degradation for charring polymers. *Polym Degrad Stab.* 2014;106:2-15. doi:10.1016/j.polymdegradstab.2013.09.022

619   14.   Courvoisier E, Bicaba Y, Colin X. Multi-scale and multi-technique analysis of
620   the thermal degradation of poly(ether ether ketone). *Polym Degrad Stab*.
621   2018;151(December 2017):65-79.
622   doi:10.1016/j.polymdegradstab.2018.03.001

623

624

6. Figures

Figure 1. TG and DTG plots of PI heated at 10 °C/min under nitrogen, 2%, 4%, 8% and 12%, and in air[2].
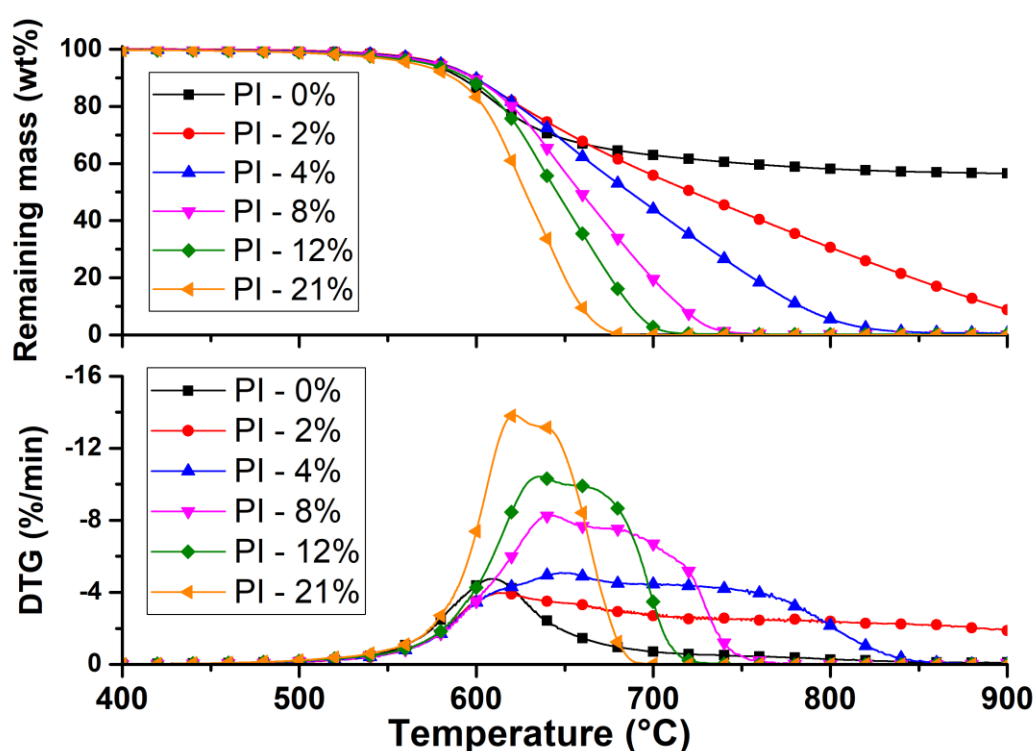

628

Figure 2. Friedman plots corresponding to a normal type of reaction (left), an accelerated reaction (middle), and a retarded reaction (right).[9]
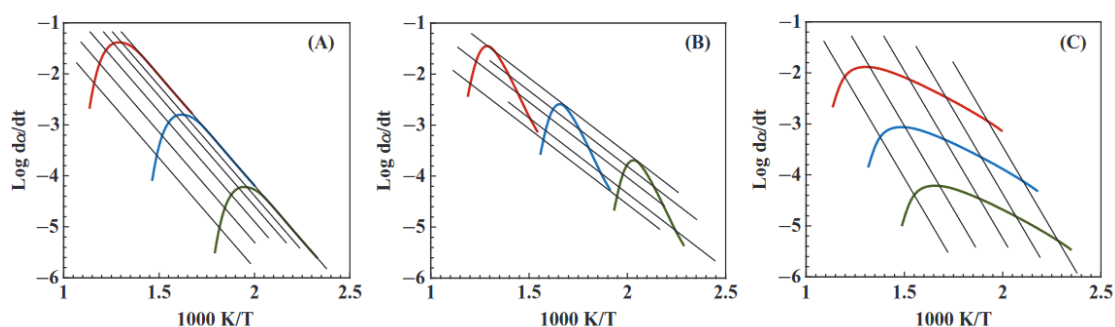
631

632

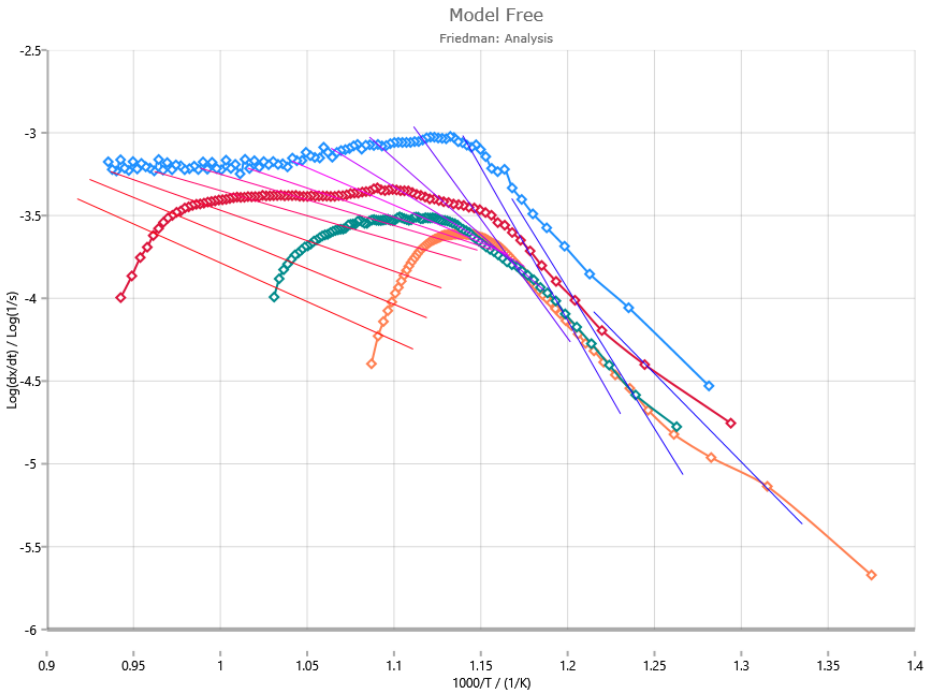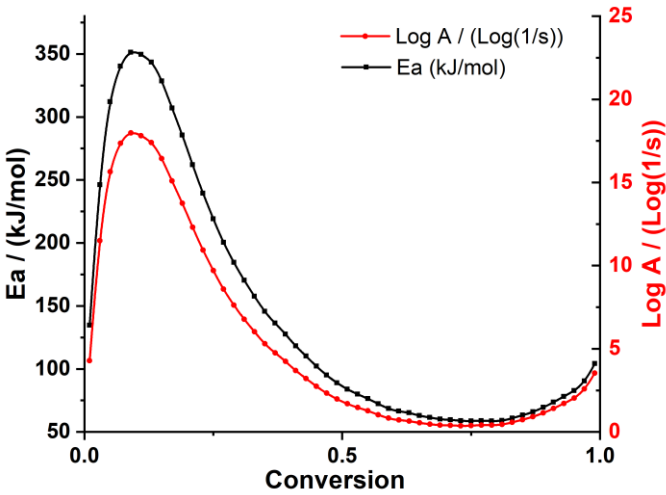**Figure 3.** TGA (left) and the corresponding DTG (right) curve of PI at 1 (black), 2
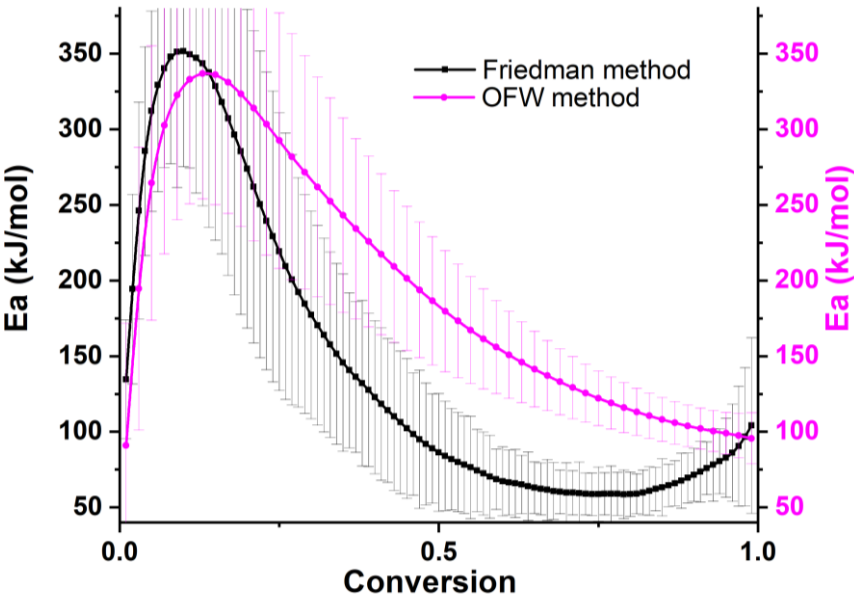(red), 5 (blue), and 10 K/min (magenta), under nitrogen.
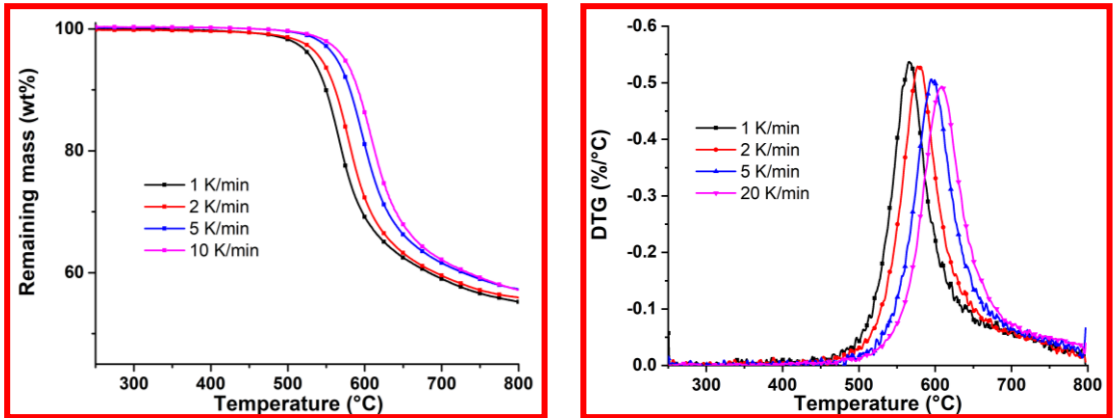
Figure 4. Friedman analysis of PI using 4 different heating rates under nitrogen
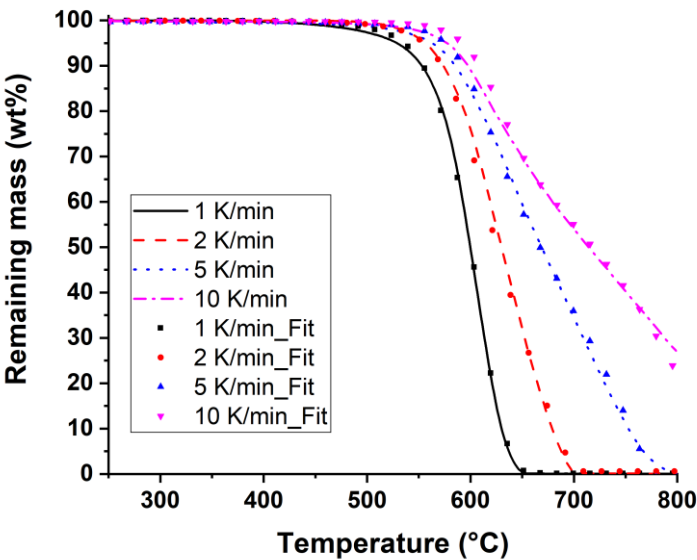(orange: 1 K/min, green: 2 K/min, red: 5 K/min, blue: 10 K/min)
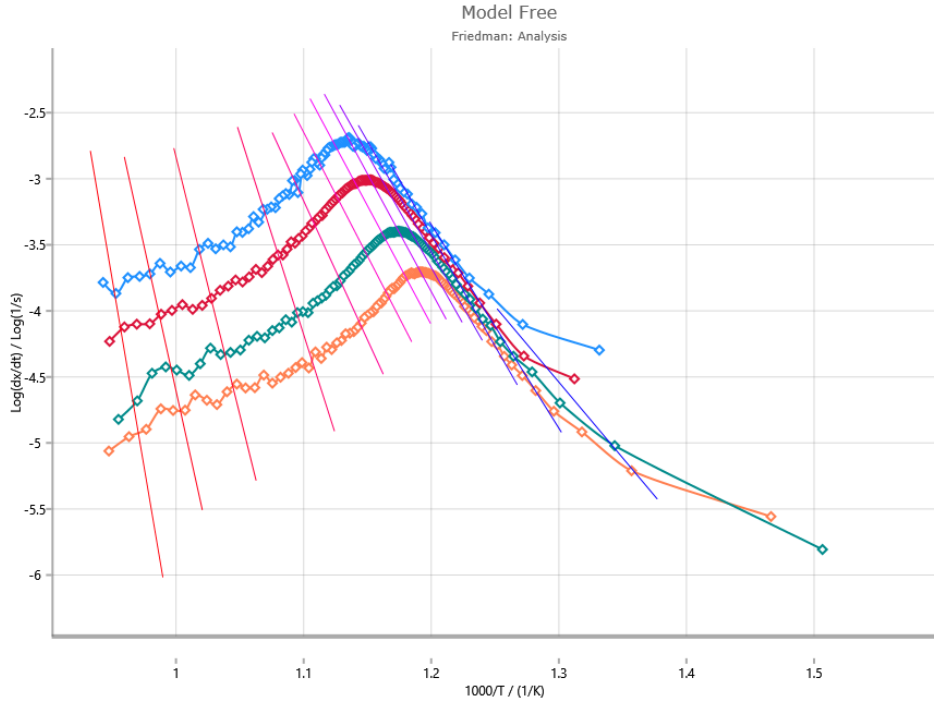
641 **Figure 5.** Activation energy plot for PI under nitrogen (left), obtained by Friedman
642 analysis
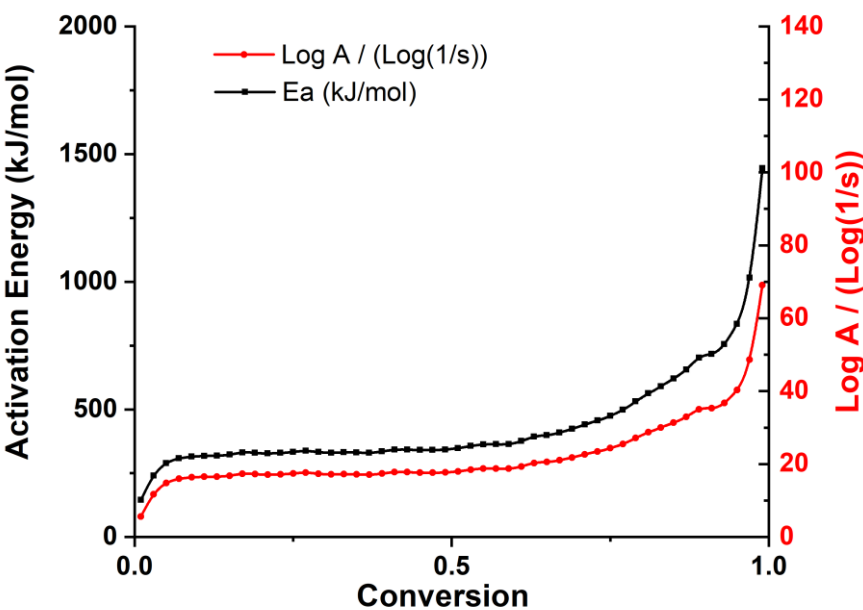
643

644 **Figure 6.** Activation energies calculated using Friedman analysis (black) and the
645 Ozawa-Flynn-Wall method (magenta) for PI under nitrogen
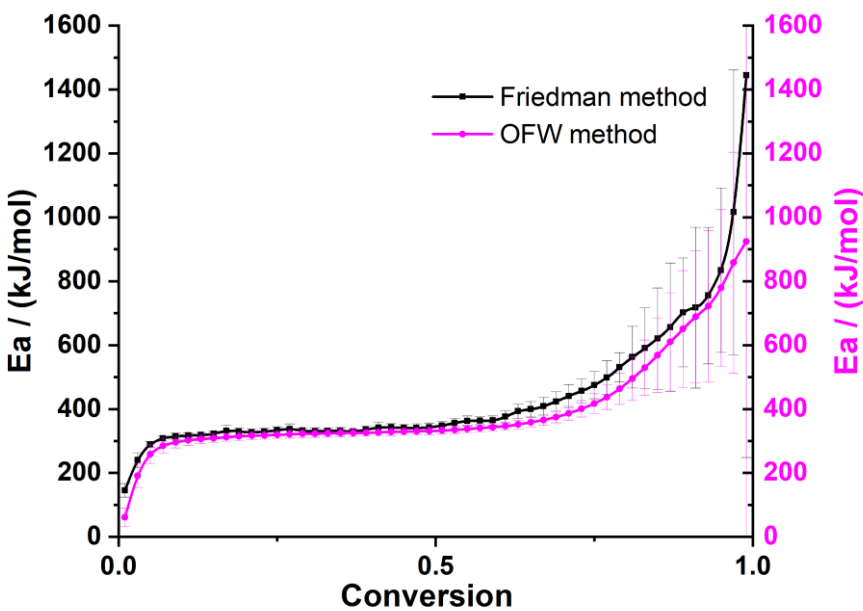
646

647

648 **Figure 7.** Best fit of the TG data for the three-stage reaction models in **Scheme 1**,
649 with the parameters given on **Scheme 1**. The curves represent the experimental
650 data and the symbols represent the model

651
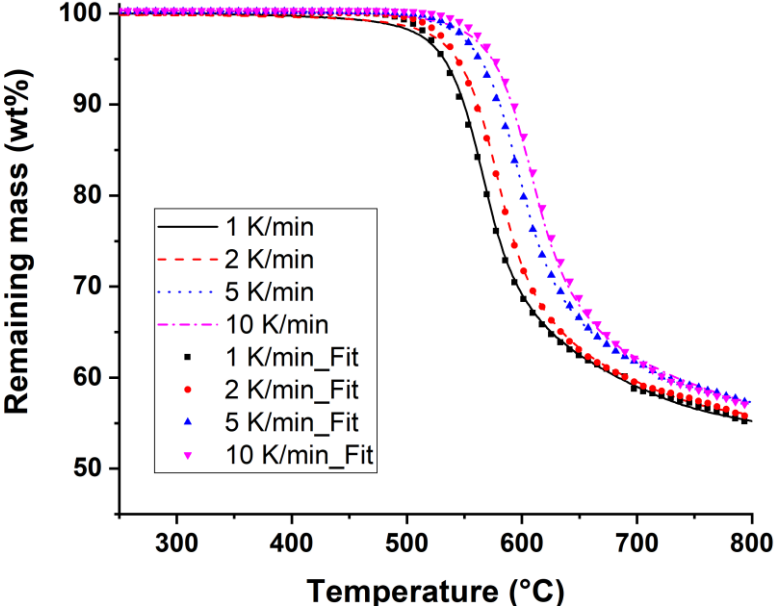
652 **Figure 8**. TGA (left) and the corresponding DTG (right) curve of PI at 1 (black), 2
653 (red) ,5 (blue), and 10 K/min (magenta), under 2% oxygen
654

655
656
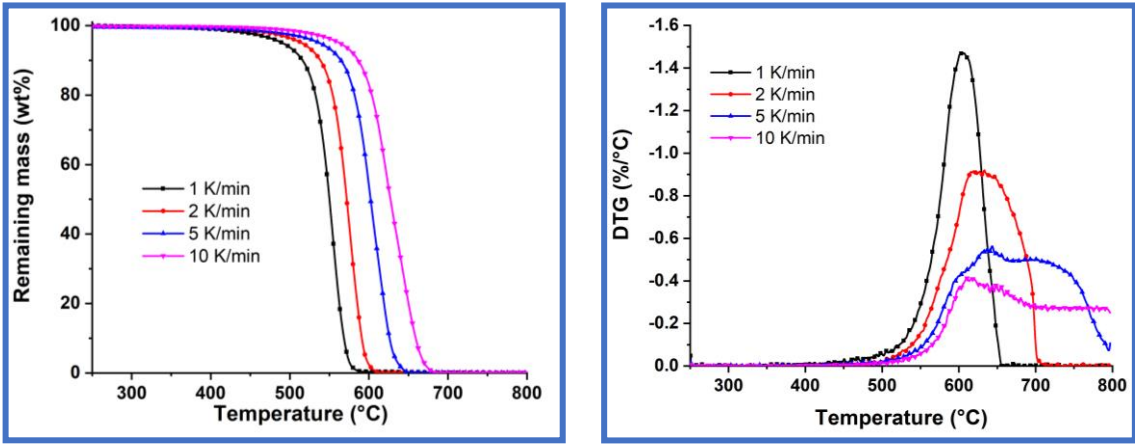
657 **Figure 9.** Friedman analysis of PI using 4 different heating rates under 2% oxygen
658   (orange: 1 K/min, green: 2 K/min, red: 5 K/min, blue: 10 K/min)

659

660 **Figure 10.** Activation energy plot for PI under 2% oxygen, obtained by Friedman
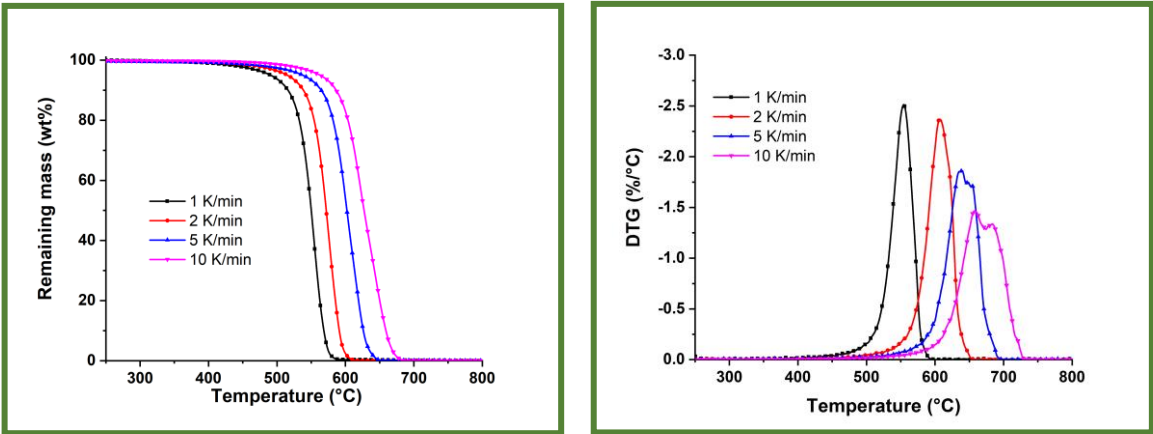661   analysis

662

663

664 **Figure 11.** Activation energies calculated using Friedman analysis (black) and the
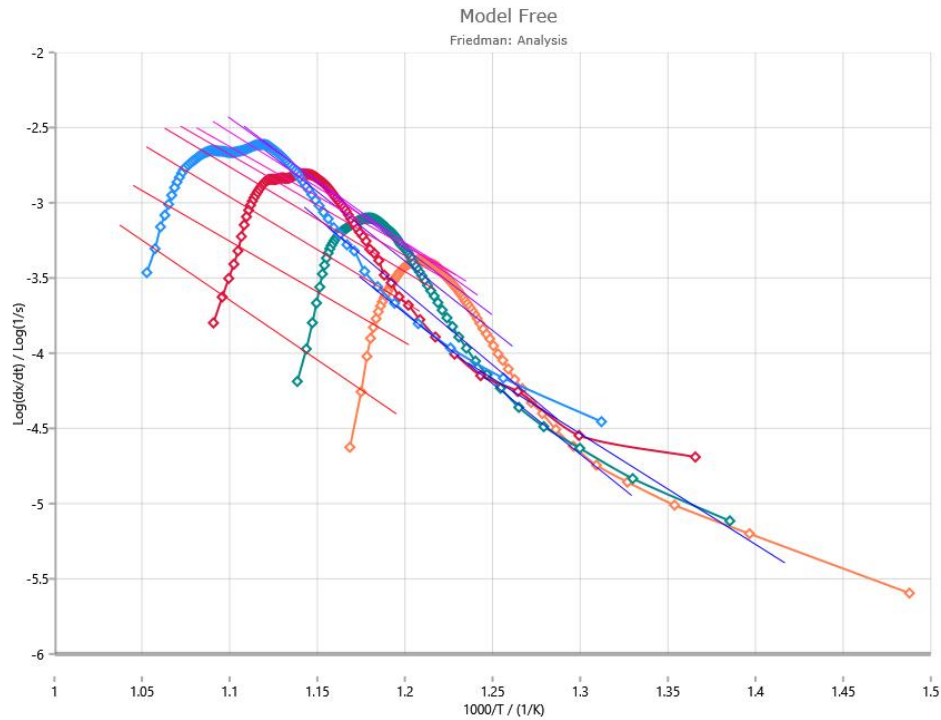665 Ozawa-Flynn-Wall method (magenta) for PI under 2% oxygen

666

667 **Figure 12.** Best fit of the TG data for the three-stage reaction models in **Scheme 2**,
668 with the parameters given on **Table 3**. The curves represent the experimental data
669 and the symbols represent the model.

670

671

672 **Figure 13.** TGA (left) and the corresponding DTG (right) curve of PI at 1 (black), 2
673 (red) ,5 (blue), and 10 K/min (magenta), in air.

674

675 **Figure 14.** Friedman analysis of PI using 4 different heating rates in air (orange: 1
676 K/min, green: 2 K/min, red: 5 K/min, blue: 10 K/min)

677
678

679 **Figure 15.** Activation energy plot for PI in air, obtained by Friedman analysis
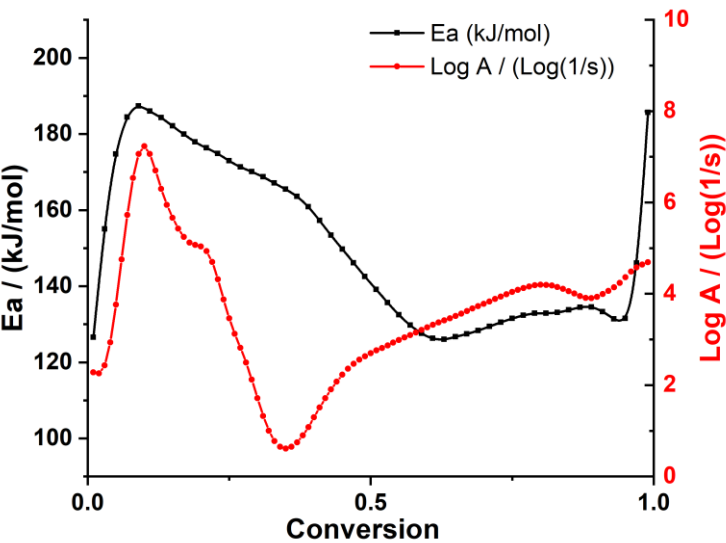
680

681 **Figure 16.** Activation energies calculated using Friedman analysis (black) and the
682 Ozawa-Flynn-Wall method (magenta) for PI in air.

683

684
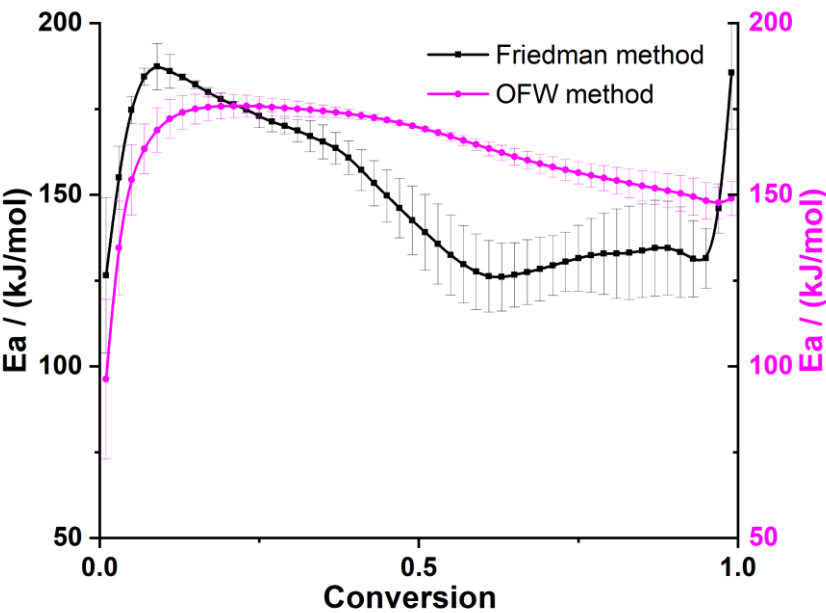
685 **Figure 17.** Best fit of the TG data for the three-stage reaction models in **Scheme 3**,
686 with the parameters given on **Table 4**. The curves represent the experimental data
687 and the symbols represent the model.
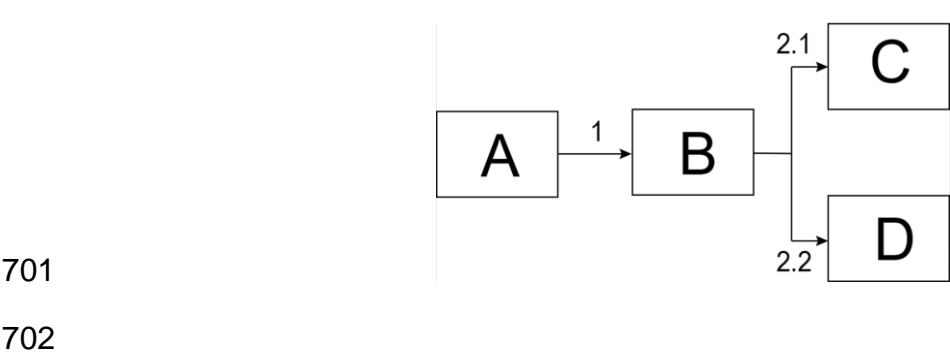

688

689
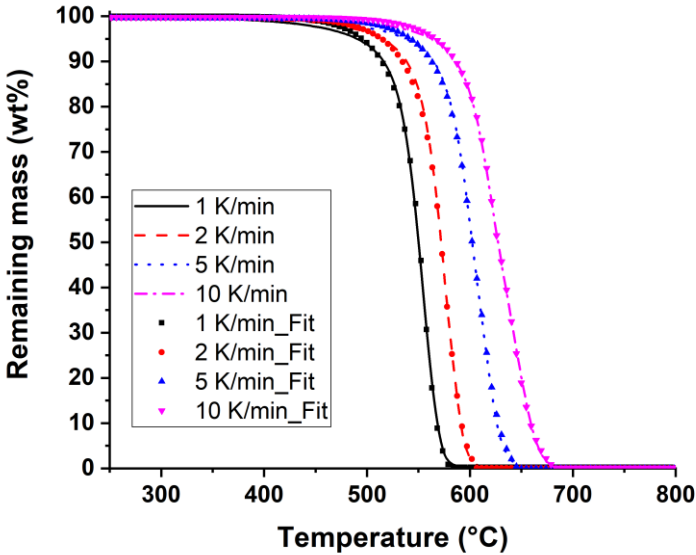
690   **Scheme 1.** Kinetic model used to model the thermal decomposition kinetics of PI
691   under nitrogen.

692

693

694
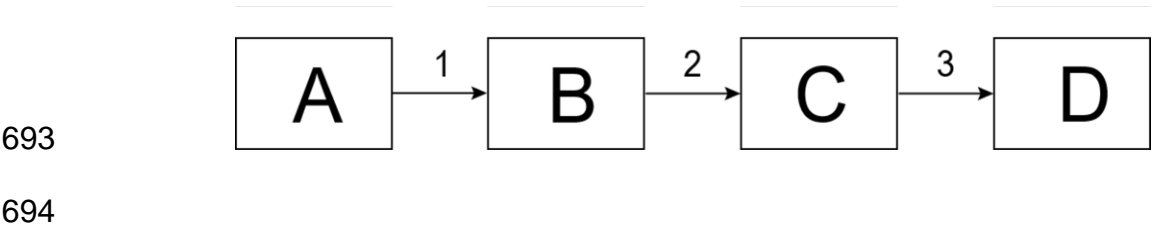
695   **Scheme 2**. Kinetic model used to model the thermal decomposition kinetics of PI
696   under 2% oxygen

697

698
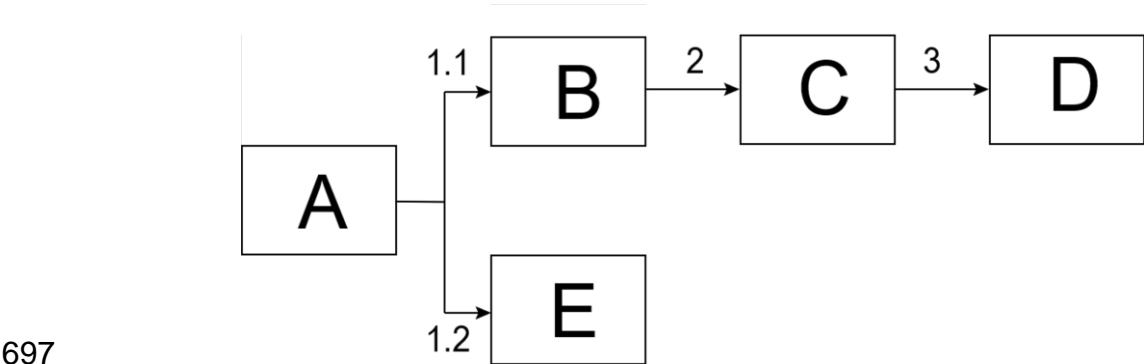
699   **Scheme 3.** Kinetic model used to model the thermal decomposition kinetics of PI in
700   air.

701

702

703 **Table 1.** Reaction types and corresponding reaction equations $d\alpha dt = -A\,eERTf(\alpha)$

Code	Function	Type of reaction
F1	$f = (1-\alpha)$	Reaction of 1st order
F2	$f = (1-\alpha)^2$	Reaction of 2nd order
Fn	$f = (1-\alpha)^n$	Reaction of nth order
R2	$f = 2(1-\alpha)^{\frac{1}{2}}$	Two-dimensional phase boundary
R3	$f = 3(1-\alpha)^{\frac{2}{3}}$	Three-dimensional phase boundary
D1	$f = \frac{1}{2}\cdot\frac{1}{\alpha}$	One-dimensional diffusion
D2	$f = -\frac{1}{\ln\big((1-\alpha)\big)}$	Two-dimensional diffusion
D3	$f = \frac{3}{2}\cdot\frac{(1-\alpha)^{\frac{2}{3}}}{1-(1-\alpha)^{\frac{1}{3}}}$	Three-dimensional diffusion Jander's type
D4	$f = \frac{3}{2}\cdot\frac{1}{\big((1-\alpha)^{\frac{1}{3}}-1\big)}$	Three-dimensional diffusion Ginstling-Brounstein type
B1	$f = (1-\alpha)\cdot\alpha$	Prout-Tompkins equation
Bna	$f = (1-\alpha)^n \cdot \alpha^{K_{cat}}$	Expanded Prout-Tompkins equation
C1	$f = (1-\alpha)\cdot(1 + K_{cat}\cdot\alpha)$	Reaction of 1st order with autocatalysis by product
Cn	$f = (1-\alpha)^n\cdot(1 + K_{cat}\cdot\alpha)$	Reaction of nth order with autocatalysis by product
Cnm	$f = (1-\alpha)^{\wedge}n\cdot(1 + K_{cat}\cdot\alpha^m)$	Reaction of nth order with m-Power autocatalysis by product
A2	$f = 2(1-\alpha)\cdot[-\ln(1-\alpha)]^{\frac{1}{2}}$	Two-dimensional nucleation according to Avrami
A3	$f = 3(1-\alpha)\cdot[-\ln(e)]^{\frac{2}{3}}$	Three-dimensional nucleation according to Avrami
An	$f = n\cdot(1-\alpha)\cdot\big[-\ln\big((1-\alpha)\big)\big]^{\frac{n-1}{n}}$	n-dimensional nucleation according to Avrami-Erofeev

705

706 **Table 2**. Kinetic parameters used in the model for the thermal decomposition of PI
707 under nitrogen

Stage (reaction type)	1 (Cna)	2 (Fn)	3 (Fn)
Ea (kJ/mol)	277.768	369.820	410.149
Log(A) (log(1/s)	14.351	20.459	23.316
Reaction order	3.000	1.593	1.708
Kcat	0.377	-	-
Contribution	0.625	0.188	0.187

708

709 **Table 3.** Kinetic parameters used in the model for the thermal decomposition of PI
710 under 2 % oxygen

Stage (reaction type)	1.1 (Fn)	1.2 (Fn)	2 (Cn)	3 (Fn)
Ea (kJ/mol)	349	353	62	99
Log(A) (log(1/s)	18.2	17.3	0.1	2.3
Reaction order	1.8	1.1	0.52	0.01
Kcat	-	-	1.69	-
Contribution	0.192	0.290	0.296	0.222

711

712

713

714 **Table 4.** Kinetic parameters used in the model for the thermal decomposition of PI
715 in air
716

Stage (reaction type)	1 (Cna)	2.1 (Cna)	2.2 (Fn)
Ea (kJ/mol)	181	122	112
Log(A) (log(1/s)	7.9	4.2	2.9
Reaction order	0.41	1.24	0.06
Kcat	0.73	0.97	-
Contribution	0.166	0.291	0.543

717